Solid State Sciences 108 (2020) 106374

Contents lists available at ScienceDirect

Solid State Sciences

journal homepage: http://www.elsevier.com/locate/ssscie

Hydrothermal synthesis and properties of $M^{II}M^{III}F_5(H_2O)_7$ ($M^{II} = Co^{2+}$ and Ni^{2+}, $M^{III} = Mn^{3+}$, Ga^{3+}, and In^{3+})

Navindra Keerthisinghe [a], Vladislav V. Klepov [a], Eric Zhang [b], Mark D. Smith [a], Shani Egodawatte [a], Stephen H. Foulger [b], Hans-Conrad zur Loye [a,*]

[a] Department of Chemistry and Biochemistry, University of South Carolina, Columbia, SC, United States
[b] Center for Optical Materials Science and Engineering Technologies (COMSET), Departments of Materials Science and Engineering & Bioengineering, Clemson University, Clemson, SC, United States

A B S T R A C T

A family of new compounds with a general formula $M^{II}M^{III}F_5(H_2O)_7$ ($M^{II} = Co^{2+}$ and Ni^{2+}, $M^{III} = Mn^{3+}$, Ga^{3+}, and In^{3+}), along with a related compound $[Ni(H_2O)_6][InF_4(H_2O)_2]_2$, was obtained via hydrothermal crystal growth and characterized using single crystal X-ray diffraction. All compounds adopt related structural motifs and differ in slight symmetry distortions rather than overall change in packing. No direct relationships between the cation size and symmetry of the crystals were found, moreover, $[Co(H_2O)_6]_2[MnF_4(H_2O)_2][MnF_6]$ that exhibits Jahn-Teller distortions of the Mn octahedra adopts the same structure as $[Ni(H_2O)_6]_2[InF_4(H_2O)_2][InF_6]$, which is lacking such distortions. Magnetic and spectroscopic properties of the former compound are also reported.

1. Introduction

Many fluorides exhibit important optical behavior, including luminescence and, in some cases, scintillation [1–5]. These properties are the result of the highly ionic nature of fluorides that are typically accompanied by a large band gap and optical transparency and, for that reason, find application as optical materials [6]. Several methods have been utilized for the synthesis of fluorides, namely solid state synthesis, subcritical solvothermal reactions, gaseous fluorination, low temperature fluorine insertion, reaction in ionic liquids, fluorolytic sol-gel synthesis and microwave-assisted routes [7–10]. Recently, the use of hydrothermal syntheses of fluorides has dominated the literature [11–18]. This approach that, moreover, yields the products in single crystal form, is easy to use and can generate high yields of phase pure products. By using HF as a solvent as well as the fluorination agent it is possible to crystallize many complex fluorides under relatively mild conditions. The effectiveness of this route has resulted in the synthesis of a variety of classes of fluorides, including inorganic fluorides, hybrid inorganic/organic materials, as well as open framework structures, such as fluorophosphates [19–25].

Hydrothermal synthesis relies on the increased solubility and product formation under temperatures in excess of the boiling point of the solution (100–500 °C). This increase in temperature as well as the high pressure changes the solubility and the increased tendency in nucleating allows for the growth of large single crystals. According to the temperature at which the reaction is carried out the hydrothermal method can be divided into three classes. In the mild hydrothermal method, where the reaction temperature ranges from 100 °C to 230 °C, a PTFE liner is used to contain the reactants and the solvents [26–30]. In moderate temperature hydrothermal reactions, the synthesis temperature can be as high as 350 °C, and supercritical hydrothermal methods operate under supercritical conditions with temperatures in excess of 374 °C [31–35]. We have found that in the mild hydrothermal regime both the reaction temperature and the dwell time significantly impact the size and the quality of the fluoride crystals obtained, where in general, as the dwell time was increased the size of these single crystals increased significantly. Herein we report the mild hydrothermal synthesis of seven complex inorganic oxyfluoride salts and their structures. Magnetic properties of one of them have been studied to probe possible magnetic interaction between the cations.

2. Experimental

2.1. Synthesis

The following materials were used as received without further purification: $Co(NO_3)_2{\cdot}6H_2O$ (Alfa Aesar, 98%), $Ni(NO_3)_2{\cdot}6H_2O$ (Alfa Aesar, Ni >19.8%), $Ga(NO_3)_3{\cdot}xH_2O$ (x ≈ 8, Sigma Aldrich, 99.9%), $In(NO_3)_3{\cdot}xH_2O$ (x ≈ 5, Alfa Aesar, 99.99%), Mn_2O_3 (Aldrich), $CoCO_3$ (Alfa Aesar, 99.5%), Tetrapropylammoniumhydroxide (TPAOH) (Sigma

* Corresponding author.
E-mail address: zurloye@mailbox.sc.edu (H.-C. zur Loye).

https://doi.org/10.1016/j.solidstatesciences.2020.106374
Received 7 June 2020; Received in revised form 23 July 2020; Accepted 25 July 2020
Available online 7 August 2020

Table 1
Reaction conditions for **1**–**4**, **6** and **7**.

Chemical formula	m($M(NO_3)_2{\cdot}xH_2O$), g	m($M(NO_3)_3{\cdot}xH_2O$), g	TPAOH, mL	HF, mL	H_2O, mL
$[Co(H_2O)_6]_2[InF_4(H_2O)_2][InF_6]$ (1)	0.291	0.376	0.5	1.0	1.0
$[Ni(H_2O)_6][GaF_5(H_2O)]$ (2)	0.290	0.319	0.5	1.0	1.0
$[Ni(H_2O)_6][InF_4(H_2O)_2]_2$ (3)	0.290	0.376	0.5	1.0	1.0
$[Ni(H_2O)_6]_2[InF_4(H_2O)_2][InF_6]$ (4)	0.290	0.376	0.5	1.0	1.0
$[Ni(H_2O)_6][GaF_5(H_2O)]$ (6)	0.290	0.319	–	1.0	1.0
$[Co(H_2O)_6][GaF_5(H_2O)]$ (7)	0.291	0.319	0.5	1.0	1.0

Aldrich, 25% in water) and HF (48%, EMD).

Caution! HF is corrosive and acutely toxic. HF exposure causes severe burns that may not be immediately painful, and may cause permanent injury or death. Appropriate personal protective equipment should be worn at all times when handling HF, and proper technique for using HF safely should always be followed.

The mild hydrothermal crystal growth technique was used to prepare all seven compounds. The syntheses were carried out in 23 mL PTFE liners that were loaded with appropriate amounts of the starting materials. Table 1 details the exact starting materials and ratios used for each reported material. The metal nitrates were placed in the PTFE liners first followed by H_2O (1 mL) and HF (1 mL). The PTFE liners were sealed inside stainless steel autoclaves that were placed inside a programmable oven. The oven was heated to 170 °C in 36 min and allowed to dwell for 72 h. After dwelling, the oven was cooled to 80 °C at a rate of 0.3 °C/min and then shut off and allowed to cool to room temperature.

$[Co(H_2O)_6]_2[MnF_4(H_2O)_2][MnF_6]$ was synthesized using the same method with slight changes of reactants and temperature profile. $CoCO_3$ (0.150 g) and Mn_2O_3 (0.159 g) were used as starting materials and were placed in 23 mL PTFE liner with the addition of 1.5 ml of HF. The autoclave containing a PTFE liner was placed in the programmable oven and heated to 200 °C in an hour and allowed to dwell for 12 h. After dwelling, the oven was shut off and allowed to cool to room temperature.

All reactions resulted in relatively large single crystals that were collected via vacuum filtration, washed with methanol, and allowed to air dry. Note that methanol was used as the solvent of choice as the crystals were soluble in water. The obtained crystals were used for single crystal X-ray diffraction and property measurements. Any remnant fluoride ions were immobilized by treating the liquid waste with excess $CaCl_2$.

2.2. Single-crystal X-ray diffraction (SXRD)

Single-crystal X-ray diffraction data were collected at 300(2) and 100 (2) K on a Bruker D8 QUEST diffractometer equipped with an Incoatec IμS 3.0 microfocus radiation source (MoKα, λ = 0.71073 Å) and a PHOTON II area detector. The crystals were mounted on a microloop using immersion oil. The raw data reduction and absorption corrections were performed using SAINT and SADABS programs [36,37]. Initial structure solutions were obtained with SHELXS-2017 using direct methods and Olex2 GUI [38]. Full-matrix least-square refinements against F [2] were performed with SHELXL software [39]. All the structures were checked for missing symmetry with the Addsym

Table 2
Crystallographic data for **1**–**7**.

Chemical formula	$[Co(H_2O)_6]_2[InF_4(H_2O)_2][InF_6]$ (1)	$[Ni(H_2O)_6][GaF_5(H_2O)]$ (2)	$[Ni(H_2O)_6][InF_4(H_2O)_2]_2$ (3)	$[Ni(H_2O)_6]_2[InF_4(H_2O)_2][InF_6]$ (4)	$[Co(H_2O)_6]_2[MnF_4(H_2O)_2][MnF_6]$ (5)	$[Ni(H_2O)_6][GaF_5(H_2O)]$ (6)	$[Co(H_2O)_6][GaF_5(H_2O)]$ (7)
Formula weight	789.72	349.54	620.51	789.28	669.96	349.54	349.76
Crystal system	Monoclinic			Triclinic			
Space group, Z	*C*2/*c*, 4	*C*2/*m*, 4	$P2_1/c$, 2	$P\bar{1}$, 1	$P\bar{1}$, 1	$P\bar{1}$, 2	$P\bar{1}$, 2
a, Å	11.1238(4)	10.8563(4)	12.6338(3)	6.61530(10)	6.42130(10)	6.4800(2)	6.4913(5)
b, Å	14.2361(5)	13.8331(5)	6.6435(2)	8.9621(2)	9.0116(2)	8.6957(3)	8.7867(7)
c, Å	13.3064(5)	6.4968(2)	9.4652(2)	8.9961(2)	9.0253(2)	8.8694(3)	8.9334(7)
α, deg.	90	90	90	102.9620(10)	104.1026(8)	103.9584(12)	104.196(2)
β, deg.	100.7280(14)	99.9610(10)	105.9184(8)	98.3470(10)	96.1201(8)	96.8177(13)	96.867(2)
γ, deg.	90	90	90	96.3110(10)	96.8142(8)	95.1076(12)	95.219(2)
V, $Å^3$	2070.37(13)	960.96(6)	763.98(3)	508.609(18)	497.936(18)	477.98(3)	486.59(7)
ρ_{calcd}, g/cm^3	2.534	2.416	2.697	2.577	2.234	2.429	2.387
Radiation (λ, Å)	MoKα, 0.71073						
μ, mm^{-1}	3.916	4.855	4.340	4.205	3.022	4.880	4.564
T, K	301(2) – 302(2)						
Crystal dim., mm^3	0.22 × 0.16 × 0.10	0.18 × 0.16 × 0.08	0.16 × 0.12 × 0.10	0.18 × 0.10 × 0.05	0.06 × 0.05 × 0.04	0.14 × 0.10 × 0.08	0.22 × 0.18 × 0.12
2θ range, deg.	2.349–42.678	2.407–40.285	3.354–45.356	2.358–45.355	2.350–29.999	2.391–37.839	2.377–37.818
Reflections collected	92165	36478	75448	57354	18749	38683	32761
Data/restraints/parameters	7499/0/189	3118/4/128	6416/0/138	8510/0/190	2882/0/183	5141/6/176	5219/6/176
R_{int}	0.0432	0.0345	0.0341	0.0352	0.0229	0.0297	0.0261
Goodness of fit	1.001	1.037	1.050	1.001	1.081	1.027	1.078
$R_1(I > 2\sigma(I))$	0.0249	0.0219	0.0190	0.0240	0.0298	0.0286	0.0280
wR_2 (all data)	0.0622	0.0553	0.0387	0.0527	0.0762	0.0614	0.0634
Largest diff. peak/hole, $e{\cdot}Å^{-3}$	1.167/-0.691	0.423/-0.391	0.768/-0.593	0.979/-1.185	0.952/-0.675	0.898/-0.614	0.819/-0.780

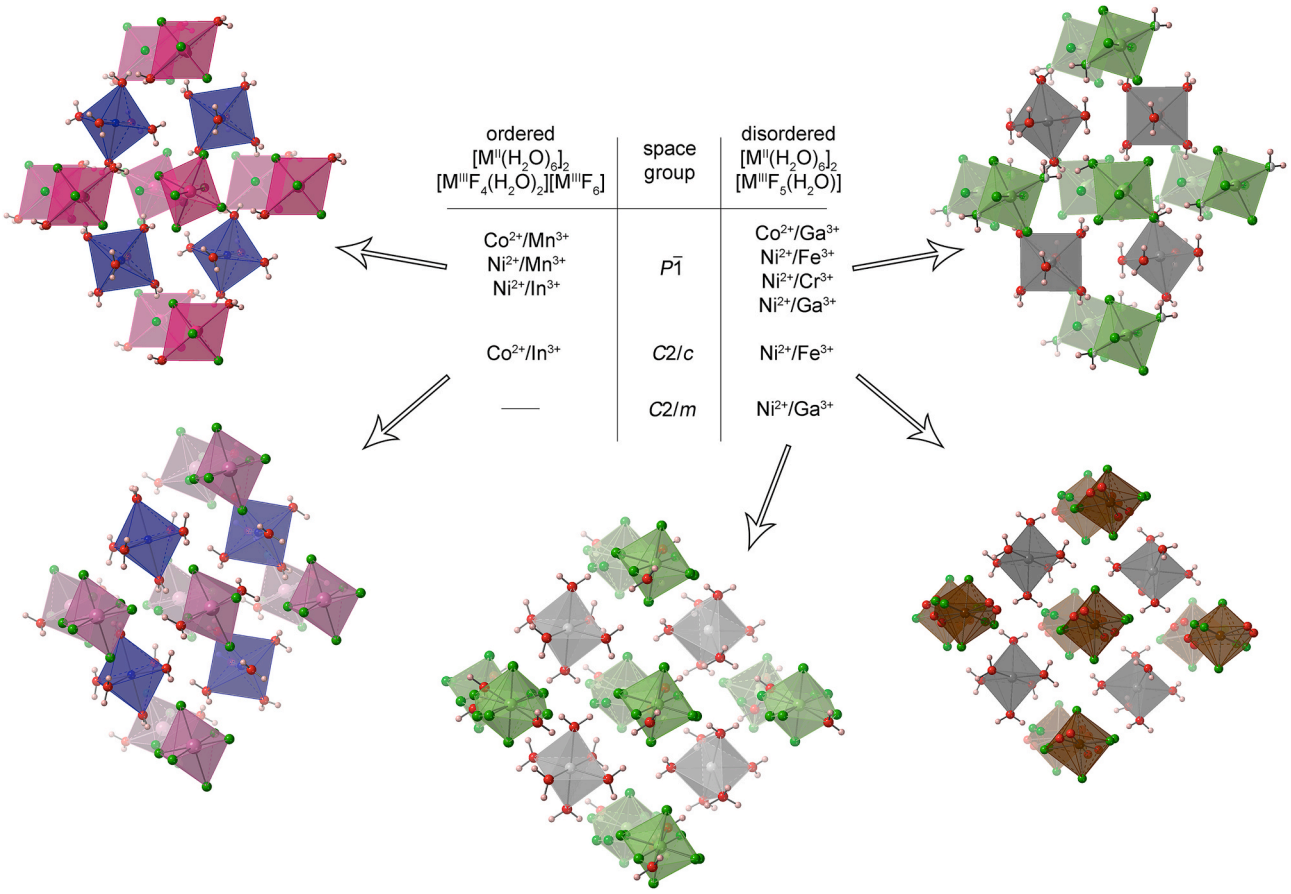

Fig. 1. The structures of the compounds $[M^{II}(H_2O)_6]_2[M^{III}F_4(H_2O)_2][M^{III}F_6] \equiv 2 \times [M^{II}(H_2O)_6][M^{III}F_5(H_2O)]$ ($M^{II} = Co^{2+}$, Ni^{2+}; $M^{III} = Cr^{3+}$, Mn^{3+}, Fe^{2+}, Ga^{3+}, In^{3+}). Mn, In, Ga, Fe, Co, and Ni polyhedra are pink, pale pink, green, brown, blue, and grey, respectively. Oxygen and fluorine atoms are red and green [49]. (For interpretation of the references to colour in this figure legend, the reader is referred to the Web version of this article.)

program implemented within PLATON software and no higher symmetry was found [40]. The crystallographic data and results of the diffraction experiments are summarized in Table 2. A detailed description of each structure solution can be found in the SI.

2.3. Powder X-ray diffraction (PXRD)

Powder X-ray diffraction (PXRD) data for phase purity confirmation were collected on polycrystalline samples ground from single crystals (Fig. S1). Data were collected on a Bruker D2 PHASER diffractometer using Cu Kα radiation over a 2θ range 10–65° with a step size of 0.02°.

2.4. Magnetic measurements

Susceptibility and magnetization measurements were performed using a Quantum Design MPMS-3 SQUID magnetometer. Susceptibility measurements were performed under an applied field of 0.1 T in the temperature range of 2–300 K. Magnetization measurements were performed at 2 K in an applied field ranging from −5 T to 5 T. All magnetic data were corrected for radial offset and shape effects [41].

2.5. Crystal chemical calculations

Crystal structure analysis was performed using the TOPOS 4.0 software package [42,43]. The method of intersecting spheres was employed for coordination number determination using the AutoCN program [44]. Dirichlet and ADS programs were employed for Voronoi-Dirichlet polyhedra construction and topological analysis, respectively. The standard structure simplification procedure was employed to obtain the underlying nets of the compounds [45].

2.6. IR spectroscopy

Vibrational spectrum over the range of 4000–650 cm^{-1} was recorded using a PerkinElmer spectrum 100 FT-IR spectrometer equipped with a diamond ATR attachment (Fig. S2).

3. Results and discussion

3.1. Crystal structure description

All seven compounds crystallize in centrosymmetric space groups, $C2/c$, $C2/m$, $P2_1/c$, and $P\bar{1}$ and, with the exception of $[Ni(H_2O)_6][InF_4(H_2O)_2]_2$, can be considered to be a variation on the same composition type $[M^{II}(H_2O)_6]_2[M^{III}F_4(H_2O)_2][M^{III}F_6] \equiv 2 \times [M^{II}(H_2O)_6][M^{III}F_5(H_2O)]$. The $[M^{III}F_5(H_2O)]^-$ complex can be either a product of the following equilibrium: $[M^{III}F_4(H_2O)_2] + [M^{III}F_6] \rightleftharpoons 2\,[M^{III}F_5(H_2O)]$, or a result of $[M^{III}F_4(H_2O)_2]^-$ and $[M^{III}F_6]^{3-}$ disorder over the same site. As single crystal X-ray diffraction shows an averaged crystal structure, no definitive conclusion can be drawn based on the present data. As there is at least one composition that shows different symmetry, i.e. $[Ni(H_2O)_6][GaF_5(H_2O)]$ that crystallizes in both $C2/m$ or $P\bar{1}$ space groups, it is likely that the symmetry of the compounds in this composition type is driven by the crystallization conditions and resulting disorder or rotations of the octahedral complexes rather than their packing. Although this conclusion seems intuitively correct, a more detailed investigation of this effect is necessary.

In six of the seven structures (Fig. 1), the metal atoms occupy

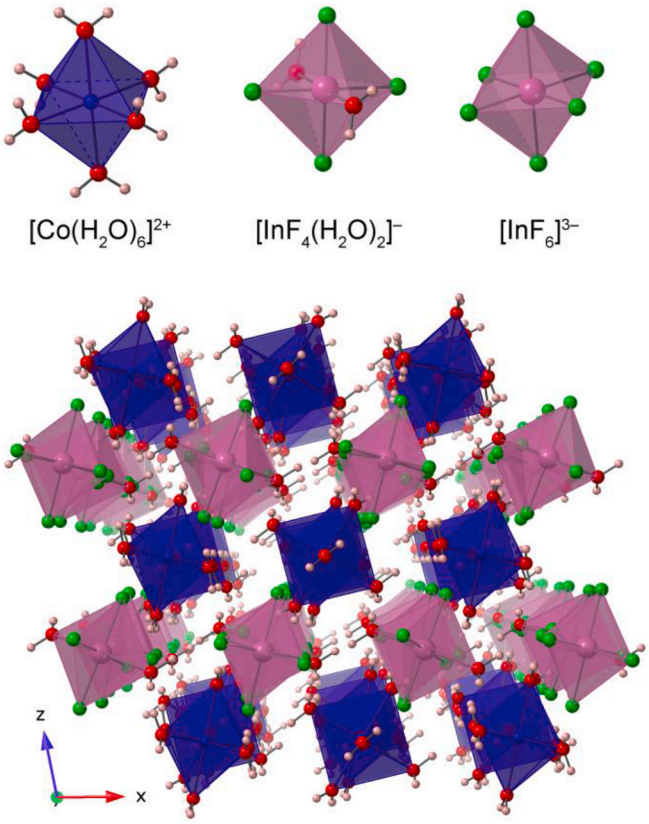

Fig. 2. (top) Coordination polyhedra and (bottom) a view on the structure of $[Co(H_2O)_6]_2[InF_4(H_2O)_2][InF_6]$ (**1**).

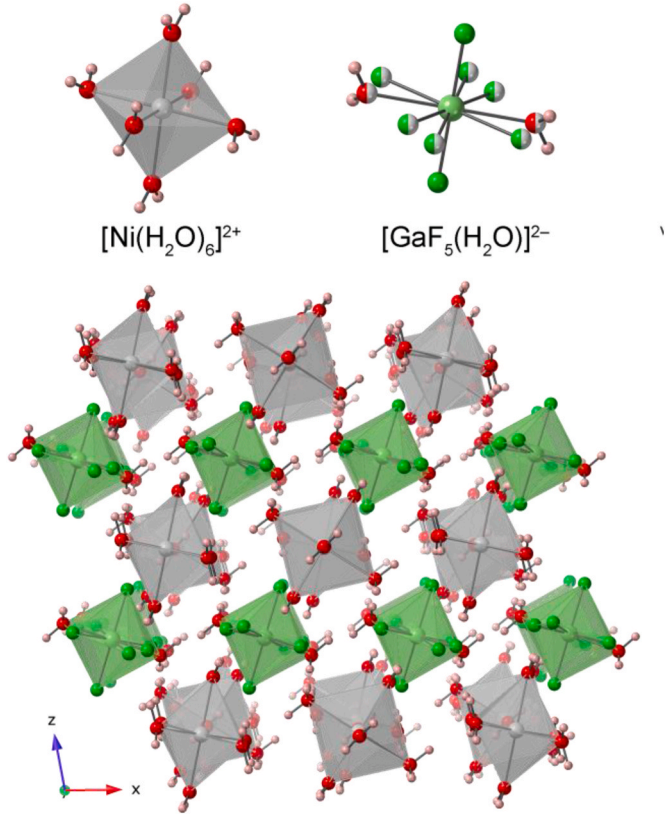

Fig. 3. (top) Coordination polyhedra and (bottom) a view on the structure of $[Ni(H_2O)_6][GaF_5(H_2O)]$ (**2**).

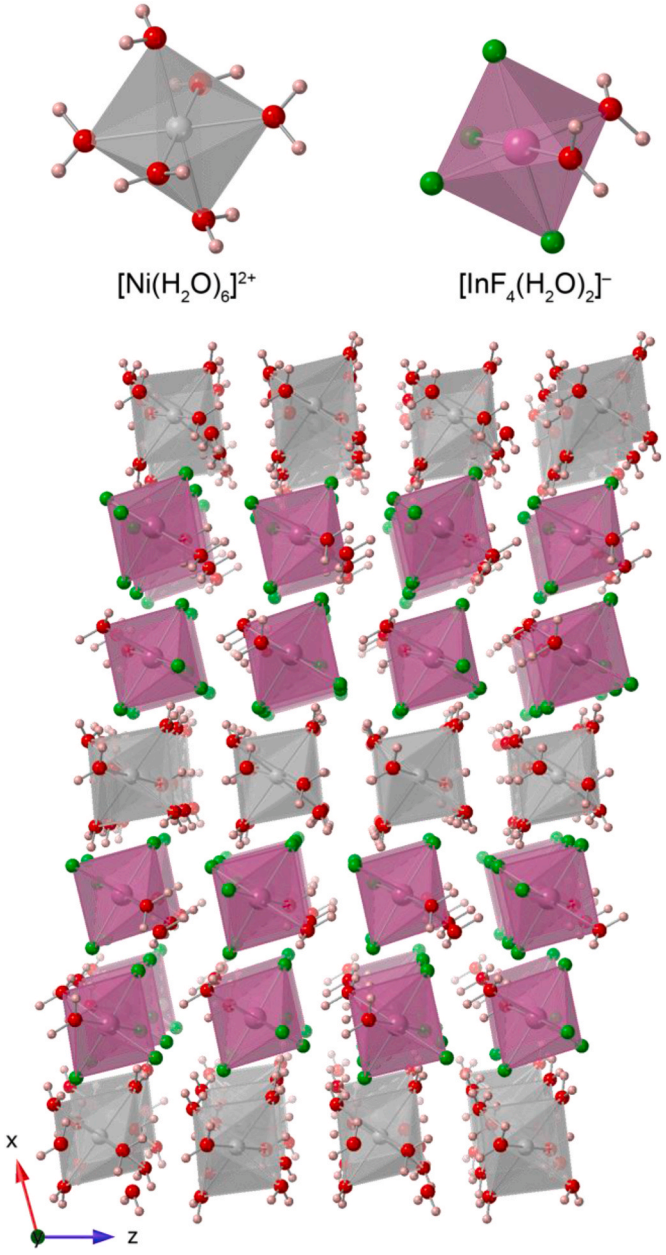

Fig. 4. (top) Coordination polyhedra and (bottom) a view on the structure of $[Ni(H_2O)_6][InF_4(H_2O)_2]_2$ (**3**).

centrosymmetric sites, In1 in $[Ni(H_2O)_6][InF_4(H_2O)_2]_2$) is the exception, and form $[MF_x(H_2O)_{6-x}]^{y+}$ complexes that bind to each other through hydrogen bonding and electrostatic interactions. The divalent Co^{2+} and Ni^{2+} cations form typical hexahydrate $[M(H_2O)_6]^{2+}$ cations [46–48]. Their positive charge is balanced by the negatively charged fluorocomplexes of the trivalent Ga^{3+}, In^{3+} and Mn^{3+} cations. The preferred fluorination of the trivalent cations is likely caused by their higher charge, and therefore stronger electrostatic interactions with the fluoride anions versus electroneutral water molecules. Due to the inversion symmetry of the *M* sites, the $[MF_5(H_2O)]^{2-}$ (or an equimolar mixture of $[MF_4(H_2O)_2]^-$ and $[MF_6]^{3-}$) complexes are disordered in the structures of $[Co(H_2O)_6][GaF_5(H_2O)]$ and both polymorphs of $[Ni(H_2O)_6][GaF_5(H_2O)]$. In all compounds, the hydrogen atoms of the water molecules participate in the formation of hydrogen bonds, which connect the metal complexes into an extended framework.

$[Co(H_2O)_6]_2[InF_4(H_2O)_2][InF_6]$ (**1**) crystallizes in the *C*2/*c* space group and contains two crystallographically unique $[Co(H_2O)_6]^{2+}$

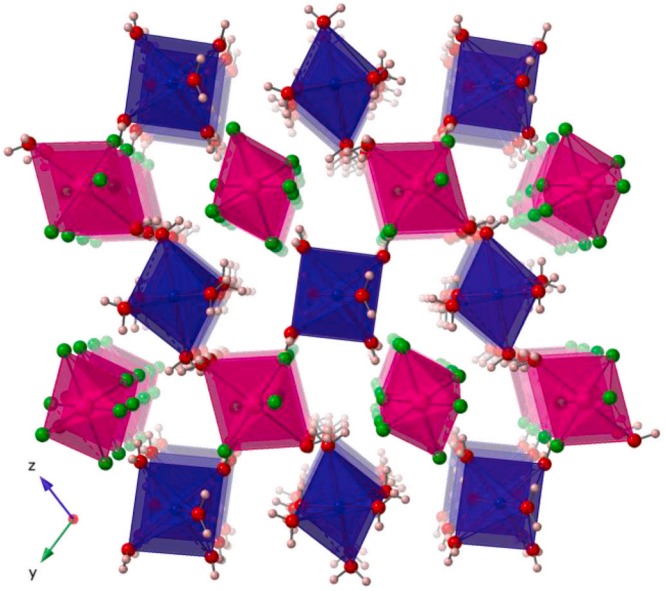

Fig. 5. A view on the structure of $[Co(H_2O)_6]_2[MnF_4(H_2O)_2][MnF_6]$. Cobalt and manganese polyhedra are shown in blue and pink. (For interpretation of the references to colour in this figure legend, the reader is referred to the Web version of this article.)

octahedra and two types of negatively charged indium complexes, $[InF_4(H_2O)_2]^-$ and $[InF_6]^{3-}$. In the former one, the two water molecules occupy *trans*-positions with In–O bond distances, 2.1463(10) and 2.1464 (10) Å, that are slightly longer than the four In–F bonds that range from 2.0337(8) to 2.0589(7) Å. The structure can be viewed as staggered pseudo layers that consist of exclusively Co or In polyhedra (Fig. 2).

$[Ni(H_2O)_6]$ $[GaF_5(H_2O)]$ (**2**) crystalizes in the monoclinic space group *C*2/*m*. Despite the different overall symmetry, this compound is also based on octahedral $[Ni(H_2O)_6]^{2+}$ cations and the disordered $[GaF_5(H_2O)]^{2-}$ anions (Fig. 3). Similar to its triclinic analog, **2** exhibits a pseudo layered structure, with layers arranged in the *ab* plane in a staggered ABAB sequence and held together via hydrogen bond interactions. The Ni–O and In–F bond distances vary over the narrow ranges of 2.0221(9)–2.0980(8) and 2.0398(7)– 2.0935(7) Å, respectively, and In–O bond length is 2.1480(8) Å.

$[Ni(H_2O)_6]$ $[InF_4(H_2O)_2]_2$ (**3**) crystalizes in the space group $P2_1/c$ and contains positively charged $[Ni(H_2O)_6]^{2+}$ octahedra and negatively charged $[InF_4(H_2O)_2]^-$ distorted octahedra. In contrast to the other structures, the two water molecules of the indium anion complex occupy cis positions. The In–O bond distances are 2.1402(7) and 2.1444(6) Å and the bond distances of the four In–F bonds vary from 2.0416(6) to 2.0876(5) Å, while the Ni–O bond distances fall into the typical range of 2.0240(6)–2.0871(6) Å. Due to the lack of fully fluorinated $[M^{III}F_6]^{3-}$ complexes in its composition, **3** shows a higher M^{III}:M^{II} molar ratio, 2:1 instead of 1:1, which results in twice as many In^{3+} pseudo layers in its structure (Fig. 4).

$[Ni(H_2O)_6]_2[InF_4(H_2O)_2]$ $[InF_6]$ and **$[Co(H_2O)_6]_2[MnF_4(H_2O)_2]$ $[MnF_6]$** (**4** and **5**) are isotypic with the previously reported triclinic zero-dimensional structure $[Ni(H_2O)_6]_2$ $[MnF_4(H_2O)_2][MnF_6]$ [49]. Both compounds crystalize in the space group $P\bar{1}$ and contain two unique Ni and Co sites that form octahedral hexaaqua complexes and two different types of In or Mn octahedral anions, $[M^{III}F_4(H_2O)_2]$ and $[M^{III}F_6]$ (M = In or Mn). The structures of these two compounds exhibit pseudo layers of successively alternating M^{II} and M^{III} octahedra layers, as shown in Fig. 5, that are held together by hydrogen bonding interactions. Both crystallographically unique nickel/cobalt cations have identical coordination with Ni–O and Co–O bond distances in the ranges of 2.0273(8)–2.0980(8) and 2.0438(16)–2.1204(15) Å, respectively. As Mn^{3+} is a *d* [4] ion and thus subject to the Jahn-Teller effect, the bond distances in the $[MnF_6]^{3-}$ and $[MnF_4(H_2O)_2]^-$ complexes are affected by a resulting tetragonal distortion. The four equatorial bonds in the $[MnF_6]^{3-}$ complex vary over the range of 1.8726(13)–1.8744(14) Å and the axial Mn–F bonds are 2.0416(15) Å. In a similar way, the Mn–F bonds distances in the $[MnF_4(H_2O)_2]^-$ complex vary over the range of 1.8413(12)–1.8341(12) Å, while the Mn–O bonds are significantly longer, 2.2250(16) Å. As expected, no such effect is observed in the $[InF_6]^{3-}$ and $[InF_4(H_2O)_2]^-$ complexes and all In–F bond distances fall into a narrow range of 2.0398(7)–2.0935(7) Å, with In–O bond distances not much longer at 2.1480(8) Å, as compared to the Mn complexe case. These compounds illustrate that the sizes of M^{II} and M^{III} do not define the symmetry of the crystals in this compositional type as two compounds with significantly different M^{II} and M^{III} cations, one exhibiting Jahn-Teller distortion and one without, can adopt the same structure.

$[Co(H_2O)_6]$ $[GaF_5(H_2O)]$ and $[Ni(H_2O)_6]$ $[GaF_5(H_2O)]$ (**6** and **7**) are isotypic and crystallize in the triclinic $P\bar{1}$ space group. In the structures of both compounds, there is one unique Co or Ni site, respectively, and two independent Ga sites. Both structures are based on pseudo layers that are shown in Fig. 6. These layers are staggered and held together by hydrogen bonding interactions. The gallium cations coordinate four fluoride anions, while two positions are half occupied by fluorine and oxygen atoms, resulting in an averaged $[GaF_5(H_2O)]^{2-}$ composition. The Co–O and Ni–O bond distances fall within narrow ranges of 2.0484(12)–2.0945(13) and 2.0152(13)–2.0783(13) Å, respectively, while the Ga–F distances range between 1.8615(11) and 1.8831(10) Å. The distances between the Ga atoms and the sites belonging to disordered F^- and H_2O are slightly longer, 1.9238(12) and 1.9800(13) Å, indicative of the presence of an electroneutral water molecule on that site.

3.2. Hydrogen bonding and molecular packing in the structures of 1–7

Electrostatic interactions and hydrogen bonds play the central role in the framework formation in the structures of **1**–**7**. While the electrostatic interactions are indirect in nature and are favored only by a dense packing of the complexes, the hydrogen bonds can favor a certain arrangement of the complexes. To reveal the connectivity in these compounds, we simplified the structures of **1**–**7** by contracting the complexes to the metal atoms and retaining the H-bond connectivity between them. Despite the difference in the symmetry of the

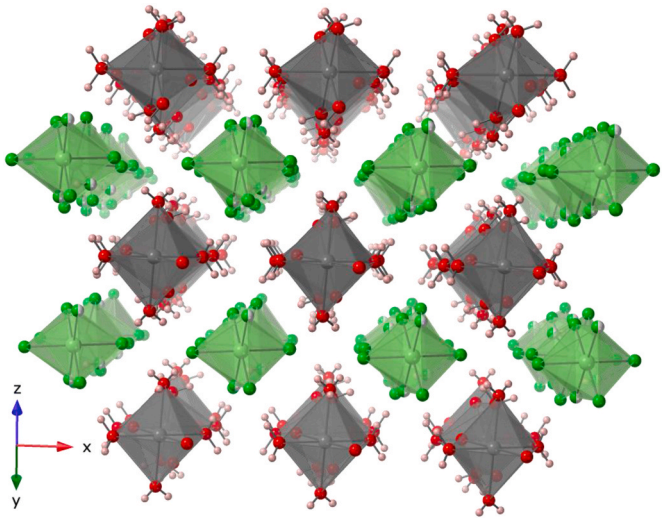

Fig. 6. A view on the structure of $[Ni(H_2O)_6][GaF_5(H_2O)]$. Nickel and gallium polyhedra are shown in grey and lime.

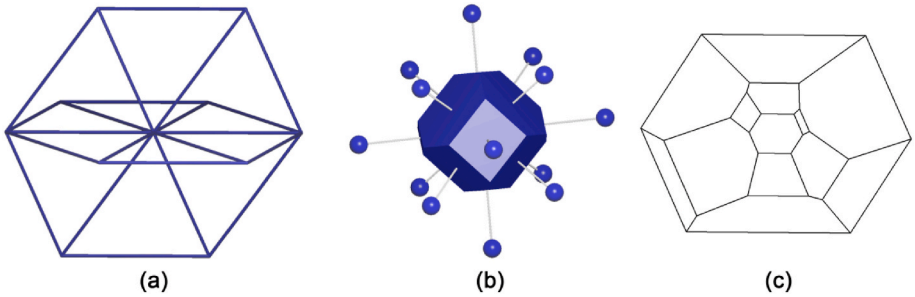

Fig. 7. (a) Node connectivity in **bct** topological type. (b and c) Voronoi polyhedra of Ni cation in the structure of $[Ni(H_2O)_6][GaF_5(H_2O)]$ (**6**) and its Shlegel diagram.

compounds, all of them, except **3**, are based on a 3-periodic uninodal (i.e. all nodes are equivalent) 10-connected net that was assigned to **bct** topological type (Fig. 7a). Compound **3** with the formula $[Ni(H_2O)_6][InF_4(H_2O)_2]_2$ has a slightly smaller number of water molecules per metal atom than the other six compounds, 3.33 vs. 3.5, indicating a decreased number of H-bond donors in **3**. Lower connectivity results in a different topology in its underlying net, which consists of two types of 9- and 10-connected nodes. To reveal the influence of the altering H-bond connectivity on the packing of the complexes, we constructed Voronoi polyhedra of the metal atoms in the metal sublattice. In all seven compounds, each metal atom forms a Voronoi polyhedron with 6 tetragonal and 8 hexagonal faces ($4^6 6^8$ combinatorial topological type, CTT) in the shape of a truncated octahedron (Fig. 7b). Although this atom arrangement is not a closest packing (but rather it corresponds to a body centered cubic packing of structural units), it is most abundant in molecular and complex structures [47,48]. Interestingly, the same packing of the octahedral molecules is observed in β-WCl_6 [50], which can be considered as the aristotype for the reported compounds.

3.3. Magnetic properties

As only one compound contains both magnetic di- and trivalent cations, $[Co(H_2O)_6]_2[MnF_4(H_2O)_2][MnF_6]$, we pursued the synthesis of its phase pure sample for magnetic measurements (Fig. 8). Although there have been reports on fluoride hydrates that exhibit signs of magnetic ordering and are built of isolated aqua- and fluorocomplexes [49], high inter-metal distances and lack of bridging atoms, which would mediate superexchange, entangles magnetic interactions in the system and reduces the chance of magnetic ordering, making one to expect a Curie-Weiss behavior with a close to zero Weiss constant for this compound. The experimental data show paramagnetic behavior over the entire temperature range, with no significant deviation from Cure-Weiss law. The inverse magnetic susceptibility plot was fitted to derive the effective magnetic moment and Weiss constant, 6.36 μ_B and −4.14 K, respectively. The effective moment is slightly higher than the moment calculated using spin-only magnetic moment, 6.24 μ_B, which indicates the presence of spin-orbit coupling on the Co^{2+} cation. Considering the Mn^{3+} cations as contributing only the spin-only moment of 3.90 μ_B, then the effective moment for the Co^{2+} cation becomes 4.05 μ_B, which agrees well with previously reported values [51].

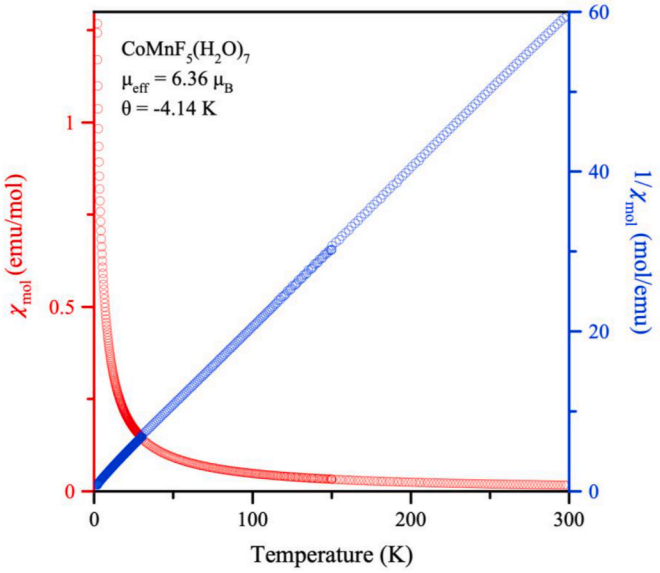

Fig. 8. Magnetic susceptibility data for $[Co(H_2O)_6]_2[MnF_4(H_2O)_2][MnF_6]$.

3.4. IR spectroscopy

The infrared spectrum of the bulk product measured from 650 to 4000 cm^{-1} revealed the expected O–H stretch and H–O–H bending bands at 3364 cm^{-1} and 1652 cm^{-1} for the water molecules that are present in the crystal structure (Fig. S2).

4. Conclusions

A series of six compounds with a general formula $[M^{II}(H_2O)_6]_2[M^{III}F_4(H_2O)_2][M^{III}F_6] \equiv 2 \times [M^{II}(H_2O)_6][M^{III}F_5(H_2O)]$ ($M^{II} = Co^{2+}$ and Ni^{2+}, $M^{III} = Mn^{3+}$, Ga^{3+}, and In^{3+}), along with a related seventh compound $[Ni(H_2O)_6][InF_4(H_2O)_2]_2$, was obtained and structurally characterized. The structures of all compounds are based on $[M^{II}(H_2O)_6]^{2+}$ cationic hexaaqua complexes and $[M^{III}F_4(H_2O)_2]^-$, $[M^{III}F_5(H_2O)]^{2-}$, and $[M^{III}F_6]^{3-}$ anionic complexes that connect into frameworks by hydrogen bonding and electrostatic interactions. All six compound have similar arrangements of the complexes in their structures; however, slight tilting and rotation of the complexes result in different symmetry of their crystals, which is likely governed by crystallization conditions. Temperature-dependent magnetic susceptibility of $[Co(H_2O)_6]_2[MnF_4(H_2O)_2][MnF_6]$ was measured to reveal paramagnetic behavior of this compound. IR spectrum of $[Co(H_2O)_6]_2[MnF_4(H_2O)_2][MnF_6]$ contains bands that correspond to stretching and bending in water molecules.

CRediT author contribution statement

Navindra Keerthisinghe: Investigation, sample synthesis, Writing - review & editing. **Vladislav V. Klepov:** Investigation, Methodology, crystal structure determination, Writing - original draft, Writing - review & editing. **Eric Zhang:** Conceptualization. **Mark D. Smith:** crystal structure determination. **Shani Egodawatte:** sample synthesis. **Stephen H. Foulger:** Conceptualization. **Hans-Conrad zur Loye:** Conceptualization, Methodology, Writing - original draft, Writing - review & editing.

Declaration of Competing interest

The authors declare that they have no known competing financial interests or personal relationships that could have appeared to influence the work reported in this paper.

Acknowledgments

This work was supported by the National Science Foundation grant number OIA-1632881.

Appendix A. Supplementary data

Supplementary data to this article can be found online at https://doi.org/10.1016/j.solidstatesciences.2020.106374.

References

[1] G. Morrison, A.M. Latshaw, N.R. Spagnuolo, H.-C. zur Loye, Observation of intense X-ray scintillation in a family of mixed anion silicates, $Cs_3RESi_4O_{10}F_2$ (RE = Y, Eu–Lu), obtained via an enhanced flux crystal growth technique, J. Am. Chem. Soc. 139 (41) (2017) 14743–14748, https://doi.org/10.1021/jacs.7b08559.

[2] C.H.L. Kennard, G. Smith, T.M. Greaney, A.H. White, Crystal structure of anhydrous barium methacrylate, J. Chem. Soc. Perkin Trans. 2 (3) (1976) 302–305, https://doi.org/10.1039/P29760000302.

[3] L.Y. Wang, E.H. Song, T.T. Deng, Y.Y. Zhou, Z.F. Liao, W.R. Zhao, B. Zhou, Q. Y. Zhang, Luminescence properties and warm white LED application of a ternary-alkaline fluoride red phosphor $K_2NaAlF_6:Mn^{4+}$, Dalton Trans 46 (30) (2017) 9925–9933, https://doi.org/10.1039/C7DT02036H.

[4] A.J. Stevenson, H. Serier-Brault, P. Gredin, M. Mortier, Fluoride materials for optical applications: single crystals, ceramics, glasses, and glass–ceramics, J. Fluor. Chem. 132 (12) (2011) 1165–1173, https://doi.org/10.1016/j.jfluchem.2011.07.017.

[5] W.W. Moses, S.E. Derenzo, Cerium fluoride, a new fast, heavy scintillator, IEEE Trans. Nucl. Sci. 36 (1) (1989) 173–176, https://doi.org/10.1109/23.34428.

[6] S.S. Perera, D.K. Amarasinghe, K.T. Dissanayake, F.A. Rabuffetti, Average and local crystal structure of β-Er:Yb:$NaYF_4$ upconverting nanocrystals probed by X-ray total scattering, Chem. Mater. 29 (15) (2017) 6289–6297, https://doi.org/10.1021/acs.chemmater.7b01495.

[7] M. Josse, M. Dubois, M. El-Ghozzi, D. Avignant, Synthesis and crystal structure of Rb2AlTb3F16: a new mixed-valence terbium fluoride, Solid State Sci 5 (8) (2003) 1141–1148, https://doi.org/10.1016/S1293-2558(03)00131-6.

[8] R. Zhang, A.S. Gibbs, W. Zhang, P.S. Halasyamani, M.A. Hayward, Structural modification of the cation-ordered ruddlesden–popper phase $YSr_2Mn_2O_7$ by cation exchange and anion insertion, Inorg. Chem. 56 (16) (2017) 9988–9995, https://doi.org/10.1021/acs.inorgchem.7b01525.

[9] E.G. Tulsky, J.R. Long, Dimensional reduction: a practical formalism for manipulating solid structures, Chem. Mater. 13 (4) (2001) 1149–1166, https://doi.org/10.1021/cm0007858.

[10] S. Wang, E.V. Alekseev, J. Diwu, H.M. Miller, A.G. Oliver, G. Liu, W. Depmeier, T. E. Albrecht-Schmitt, Functionalization of borate networks by the incorporation of fluoride: syntheses, crystal structures, and nonlinear optical properties of novel actinide fluoroborates, Chem. Mater. 23 (11) (2011) 2931–2939, https://doi.org/10.1021/cm2004984.

[11] V.V. Klepov, J.B. Felder, H.-C. zur Loye, Synthetic strategies for the synthesis of ternary uranium(IV) and thorium(IV) fluorides, Inorg. Chem. 57 (9) (2018) 5597–5606, https://doi.org/10.1021/acs.inorgchem.8b00570.

[12] J. Felder, J. Yeon, M. Smith, H.-C. zur Loye, Application of a mild hydrothermal method to the synthesis of mixed transition-metal(ii)/Uranium(iv) fluorides, Inorg Chem Front 4 (2) (2017) 368–377, https://doi.org/10.1039/C6QI00491A.

[13] A.T. Chemey, J.M. Sperling, T.E. Albrecht-Schmitt, Expanding pentafluorouranates: hydrothermal synthesis and characterization of β-$NaUF_5$ and β-$NaUF_5 \cdot H_2O$, RSC Adv 8 (50) (2018) 28642–28648, https://doi.org/10.1039/C8RA05780J.

[14] J.C. Hancock, M.L. Nisbet, W. Zhang, P.S. Halasyamani, K.R. Poeppelmeier, Periodic tendril perversion and helices in the $AMoO_2F_3$ (A = K, Rb, NH_4, Tl) family, J. Am. Chem. Soc. 142 (13) (2020) 6375–6380, https://doi.org/10.1021/jacs.0c01218.

[15] J. Yeon, J.B. Felder, M.D. Smith, G. Morrison, H.-C. zur Loye, Synthetic strategies for new vanadium oxyfluorides containing novel building blocks: structures of V(iv) and V(v) containing $Sr_4V_3O_5F_{13}$, $Pb_7V_4O_8F_{18}$, $Pb_2VO_2F_5$, and Pb_2VOF_6, CrystEngComm 17 (44) (2015) 8428–8440, https://doi.org/10.1039/C5CE01464F.

[16] C.J. Windorff, A.T. Chemey, J.M. Sperling, B.E. Klamm, T.E. Albrecht-Schmitt, Examination of molten salt reactor relevant elements using hydrothermal synthesis, Inorg. Chem. 59 (7) (2020) 4176–4180, https://doi.org/10.1021/acs.inorgchem.0c00360.

[17] P.M. Almond, L. Deakin, A. Mar, T.E. Albrecht-Schmitt, Hydrothermal synthesis, structure, and magnetic properties of a layered organically templated uranium aquofluoride: $[C_5H_{14}N_2][U_2F_{10}(H_2O)]$, Inorg. Chem. 40 (5) (2001) 886–890, https://doi.org/10.1021/ic000921a.

[18] C.D. McMillen, J.W. Kolis, Hydrothermal synthesis as a route to mineralogically-inspired structures, Dalton Trans 45 (7) (2016) 2772–2784, https://doi.org/10.1039/C5DT03424H.

[19] L. Beitone, J. Marrot, T. Loiseau, G. Férey, M. Henry, C. Huguenard, A. Gansmuller, F. Taulelle, MIL-50, an open-framework GaPO with a periodic pattern of small water ponds and dry rubidium atoms: a combined xrd, NMR, and computational study, J. Am. Chem. Soc. 125 (7) (2003) 1912–1922, https://doi.org/10.1021/ja029072b.

[20] R.E. Morris, A. Burton, L.M. Bull, S.I. Zones, SSZ-51A new aluminophosphate zeotype: synthesis, crystal structure, NMR, and dehydration properties, Chem. Mater 16 (15) (2004) 2844–2851, https://doi.org/10.1021/cm0353005.

[21] N. Simon, J. Marrot, T. Loiseau, G. Férey, Hydrothermal synthesis and crystal structures of two open-framework fluorinated aluminum phosphates templated by 1,3-diaminopropane (ULM-4 & MIL-64), Solid State Sci 8 (11) (2006) 1361–1367, https://doi.org/10.1016/j.solidstatesciences.2006.07.004.

[22] A.C. Bean, T.A. Sullens, W. Runde, T.E. Albrecht-Schmitt, Hydrothermal preparation of nickel(II)/Uranium(IV) fluorides with one-, two-, and three-dimensional topologies, Inorg. Chem. 42 (8) (2003) 2628–2633, https://doi.org/10.1021/ic0262076.

[23] M.A. AlDamen, H.K. Juwhari, A.M. Al-zuheiri, L.A. Alnazer, Hydrothermal synthesis, crystal structure, and photoluminescent properties of Li[UO2(CH3COO)3]3[Co(H2O)6], Crystallogr. Rep. 62 (7) (2017) 1160–1164, https://doi.org/10.1134/S1063774517070021.

[24] A.T. Chemey, J.M. Sperling, C.J. Windorff, D.E. Hobart, T.E. Albrecht-Schmitt, Structural relationships and absorption spectroscopy of β-$[NH_4][UF_5]$ and $[NH_4][Pu_3F_{13}]$, Cryst. Growth Des 20 (5) (2020) 2998–3006, https://doi.org/10.1021/acs.cgd.9b01642.

[25] A.T. Chemey, T.E. Albrecht-Schmitt, Redetermination of the crystal structure of tetralithium octafluoridozirconate(IV), Li_4ZrF_8, from single-crystal X-ray data, Acta Crystallogr. Sect. E Crystallogr. Commun. 75 (2) (2019) 139–141, https://doi.org/10.1107/S2056989018018194.

[26] V.V. Klepov, K.A. Pace, S. Calder, J.B. Felder, H.-C. Loye, zur. 3d-Metal Induced Magnetic Ordering on U(IV) Atoms as a Route toward U(IV) Magnetic Materials, J. Am. Chem. Soc. 141 (9) (2019) 3838–3842, https://doi.org/10.1021/jacs.9b00345.

[27] G.B. Ayer, V.V. Klepov, M.D. Smith, H.-C. zur Loye, Mild hydrothermal synthesis of the complex hafnium-containing fluorides $Cs_2[M(H_2O)_6][Hf_2F_{12}]$ (M = Ni, Co, Zn), $CuHfF_6(H_2O)_4$, and $Cs_2Hf_3Mn_3F_{20}$ based on HfF_7 and HfF_6 coordination polyhedra, Inorg. Chem. 58 (19) (2019) 13049–13057, https://doi.org/10.1021/acs.inorgchem.9b01958.

[28] G.B. Ayer, V.V. Klepov, K.A. Pace, H.-C. zur Loye, Quaternary cerium(iv) containing fluorides exhibiting Ce_3F_{16} sheets and Ce_6F_{30} frameworks, Dalton Trans 49 (18) (2020) 5898–5905, https://doi.org/10.1039/D0DT00616E.

[29] V.V. Klepov, G. Morrison, H.-C. Loye, zur. $Na_nMTh_6F_{30}$: a Large Family of Quaternary Thorium Fluorides, *Cryst. Growth Des.* 19 (2) (2019) 1347–1355, https://doi.org/10.1021/acs.cgd.8b01742.

[30] R.E. Sykora, M. Ruf, T.E. Albrecht-Schmitt, Organically templated zirconium fluorides: hydrothermal syntheses, structural relationships, and thermal behavior of (C2H10N2)Zr2F10·H2O and (C4H12N2)ZrF6·H2O, J. Solid State Chem. 159 (1) (2001) 198–203, https://doi.org/10.1006/jssc.2001.9151.

[31] Pace, K. A.; Klepov, V. V.; Morrison, G.; Zur Loye, H.-C. Moderate Supercritical Synthesis as a Facile Route to Mixed-Valent Uranium(Iv,. v) v vi, Silicates. *Chem. Commun.* 54 (98) (2018) 13794–13797, https://doi.org/10.1039/C8CC07789D.

[32] K.A. Pace, V. Kocevski, S.G. Karakalos, G. Morrison, T. Besmann, H.-C. zur Loye, Na $_2(UO_2)(BO_3)$: an all-uranium(V) borate synthesized under mild hydrothermal conditions, Inorg. Chem. 57 (8) (2018) 4244–4247, https://doi.org/10.1021/acs.inorgchem.8b00487.

[33] T.M. Smith Pellizzeri, M.A. McGuire, C.D. McMillen, Y. Wen, G. Chumanov, J. W. Kolis, Two halide-containing cesium manganese vanadates: synthesis, characterization, and magnetic properties, Dalton Trans 47 (8) (2018) 2619–2627, https://doi.org/10.1039/C7DT04642A.

[34] L.D. Sanjeewa, C.D. McMillen, M.A. McGuire, J.W. Kolis, Manganese vanadate chemistry in hydrothermal BaF_2 brines: $Ba_3Mn_2(V_2O_7)_2F_2$ and $Ba_7Mn_8O_2(VO_4)_2F_{23}$, Inorg. Chem. 55 (24) (2016) 12512–12515, https://doi.org/10.1021/acs.inorgchem.6b02355.

[35] C.C. Underwood, M. Mann, C.D. McMillen, J.W. Kolis, Hydrothermal descriptive chemistry and single crystal structure determination of cesium and rubidium thorium fluorides, Inorg. Chem. 50 (22) (2011) 11825–11831, https://doi.org/10.1021/ic2019555.

[36] Saint, Bruker, AXS Inc., Madison, Wisconsin, USA, 2012.

[37] L. Krause, R. Herbst-Irmer, G.M. Sheldrick, D. Stalke, Comparison of silver and molybdenum microfocus X-ray sources for single-crystal structure determination, J. Appl. Crystallogr. 48 (1) (2015) 3–10, https://doi.org/10.1107/S1600576714022985.

[38] O.V. Dolomanov, L.J. Bourhis, R.J. Gildea, J.A.K. Howard, H. Puschmann, OLEX2: a complete structure solution, refinement and analysis program, J. Appl. Crystallogr. 42 (2) (2009) 339–341.

[39] G.M. Sheldrick, Crystal structure refinement with *SHELXL*, Acta Crystallogr. Sect. C Struct. Chem. 71 (1) (2015) 3–8, https://doi.org/10.1107/S2053229614024218.

[40] A. Spek, Structure validation in chemical crystallography, Acta Crystallogr. D 65 (2) (2009) 148–155.

[41] G. Morrison, H.-C. zur Loye, Simple correction for the sample shape and radial offset effects on SQUID magnetometers: magnetic measurements on ln 2 O 3 (ln =Gd, Dy, Er) standards, J. Solid State Chem. 221 (2015) 334–337, https://doi.org/10.1016/j.jssc.2014.10.026.

[42] V.A. Blatov, A.P. Shevchenko, V.N. Serezhkin, *TOPOS* 3.2: a new version of the program package for multipurpose crystal-chemical analysis, J. Appl. Crystallogr. 33 (4) (2000), https://doi.org/10.1107/S0021889800007202, 1193–1193.

[43] V.A. Blatov, Multipurpose crystallochemical analysis with the program package TOPOS, IUCr CompComm Newslett 7 (2006) 4.

[44] V.A. Blatov, V.N. Serezhkin, Stereoatomic model of the structure of inorganic and coordination compounds, Russ. J. Inorg. Chem. 45 (2000) S105–S222.

[45] V.A. Blatov, A.P. Shevchenko, D.M. Proserpio, Applied topological analysis of crystal structures with the program package ToposPro, Cryst. Growth Des. 14 (7) (2014) 3576–3586, https://doi.org/10.1021/cg500498k.
[46] A.J. Locock, P.C. Burns, T.M. Flynn, Divalent transition metals and magnesium IN structures that contain the autunite-type sheet, Can. Mineral. 42 (6) (2004) 1699–1718, https://doi.org/10.2113/gscanmin.42.6.1699.
[47] V.V. Klepov, L.B. Serezhkina, V.N. Serezhkin, E.V. Alekseev, Synthesis and crystal structure analysis of uranyl triple acetates, J. Solid State Chem. 244 (2016) 100–107, https://doi.org/10.1016/j.jssc.2016.09.019.
[48] V.V. Klepov, E.V. Peresypkina, L.B. Serezhkina, M.O. Karasev, A.V. Virovets, V. N. Serezhkin, Crystal structure of [M(H2O)6][UO2(CH3COO)3]2 (M = Mg2+, Co2 + and Zn2+), Polyhedron 61 (2013) 137–142, https://doi.org/10.1016/j.poly.2013.05.048, 0.
[49] J.B. Felder, M.D. Smith, A. Sefat, H.-C. zur Loye, Magnetic and thermal behavior of a family of compositionally related zero-dimensional fluorides, Solid State Sci 81 (2018) 19–25, https://doi.org/10.1016/j.solidstatesciences.2018.04.014.
[50] F. Tamadon, K. Seppelt, The elusive halides VCl $_5$, MoCl $_6$, and ReCl $_6$, Angew. Chem. Int. Ed. 52 (2) (2013) 767–769, https://doi.org/10.1002/anie.201207552.
[51] J. Yeon, M.D. Smith, J. Tapp, A. Möller, H.-C. zur Loye, Application of a mild hydrothermal approach containing an in situ reduction step to the growth of single crystals of the quaternary U(IV)-Containing fluorides Na4MU6F30 (M = Mn2+, Co2+, Ni2+, Cu2+, and Zn2+) crystal growth, structures, and magnetic properties, J. Am. Chem. Soc. 136 (10) (2014) 3955–3963, https://doi.org/10.1021/ja412725r.